International Journal of Heat and Mass Transfer 135 (2019) 985–995

Contents lists available at ScienceDirect

International Journal of Heat and Mass Transfer

journal homepage: www.elsevier.com/locate/ijhmt

Experimental and numerical investigation of smoke dynamics in vertical cylinders and open-air environment

Chan-Sol Ahn [a,b,1], Chan-Woo Park [a,1], Min-Woo Kim [a], Tae-Gun Kim [a], Scott C. James [c], Youngbin Yoon [d], Alexander L. Yarin [e,*], Sam S. Yoon [a,*]

[a] School of Mechanical Engineering, Korea University, Seoul 136-713, Republic of Korea
[b] Fire Research Center, Korea Institute of Civil Engineering and Building Technology, 283, Goyang-daero, Ilsanseo-gu, 10223 Goyang-si, Republic of Korea
[c] Depts. of Geosciences and Mech. Eng., Baylor University, Waco, TX 76798, USA
[d] Department of Mechanical and Aerospace Engineering, Seoul National University, Seoul 08826, Republic of Korea
[e] Department of Mechanical & Industrial Engineering, University of Illinois at Chicago, 842 W. Taylor St., Chicago 60607, USA

ARTICLE INFO

Article history:
Received 23 November 2018
Received in revised form 13 February 2019
Accepted 14 February 2019

Keywords:
Smoke dynamics
Turbulent buoyant plume
Wall effects
Confined environments

ABSTRACT

Smoke rise in elevator shafts and stairwells is a primary risk from fires. Information on temperature and smoke velocity is necessary for safety evaluation and evacuation guidelines when designing high-rise buildings. Small-scale experiments were performed to measure smoke rise in open-ended, 2-m cylinders with diameters $D = 1$, 0.5, and 0.14 m and heating powers $Q_z = 32$, 144, and 220 W. When $D \geq 0.5$ m, smoke characteristics resembled those under open-air conditions for all values of Q_z with minor deviations. When $D = 0.14$ m, smoke velocity decreased due to the increased relative boundary-layer thickness. For this narrowest cylinder, smoke temperature also decreased because of the relative increase of cool air drawn through the cylinder bottom. The overall mass flow rate was lowest through the smallest cylinder because of the reduced axial velocity and cross-sectional diameter. The axial velocity became fully developed toward the cylinder top; however, the velocity decreased again when the smoke exited. Temperature distributions were also uniform at the cylinder outlet because of the fully developed flow field. Increase in Q_z increased temperature and velocity for all cylinders. Both the analytical solution from the open-air plume theory and numerical simulations using Fire Dynamics Simulator were compared against experimental data.

1. Introduction

Understanding smoke dynamics in narrow, vertical shafts is of critical importance to the safety evaluation and design of high-rise buildings. Furthermore, thermal buoyant forces drive the upward flow of air in what is known as the "stack effect." As warm air rises, it is replaced by laterally inflowing cool air. The stack effect increases convective heat loss driving up heating, ventilation, and air conditioning costs. If there is a building fire, the stack effect forces toxic smoke up elevator shafts or stairwells to threaten occupants on higher floors as depicted in Fig. 1a. Understanding the thermo-physical properties of smoke plumes is required to optimize the design of evacuation routes. Smoke dynamics depend on the fire size, ambient conditions, and building geometry. This has motivated the study of smoke dynamics as a function of fire intensity and the confining geometry.

There are many studies of pool fires in both unconfined (open-air) and confined environments. Velocities, temperatures, and volumetric flowrates of smoke from an open-air pool fire have been described by self-similar plume theory [1–16]. However, because fires often occur in confined spaces, smoke dynamics in a "compartment" have also attracted significant attention [17–23]. In a compartment (room) fire, smoke rises to the ceiling, but if the opportunity exists, it will enter a vertical shaft and spread to upper floors in an "L-shaped" configuration [24–27]. Compartments with large height-to-width ratios include elevator shafts and stairwells and it is these systems that are approximated with the cylinders studied here as illustrated in Fig. 1b.

There are several numerical and experimental studies of smoke dynamics in L-shaped configurations [24–27]. Comparing simulations in an L-shaped system, Zhang et al. [28] emphasized the importance of entrainment rates. Zhang et al. [29] predicted that the locations where pressure inside the shaft was equal to the

* Corresponding authors.
E-mail addresses: ayarin@uic.edu (A.L. Yarin), skyoon@korea.ac.kr (S.S. Yoon).
[1] These authors contributed equally.

https://doi.org/10.1016/j.ijheatmasstransfer.2019.02.046
0017-9310/

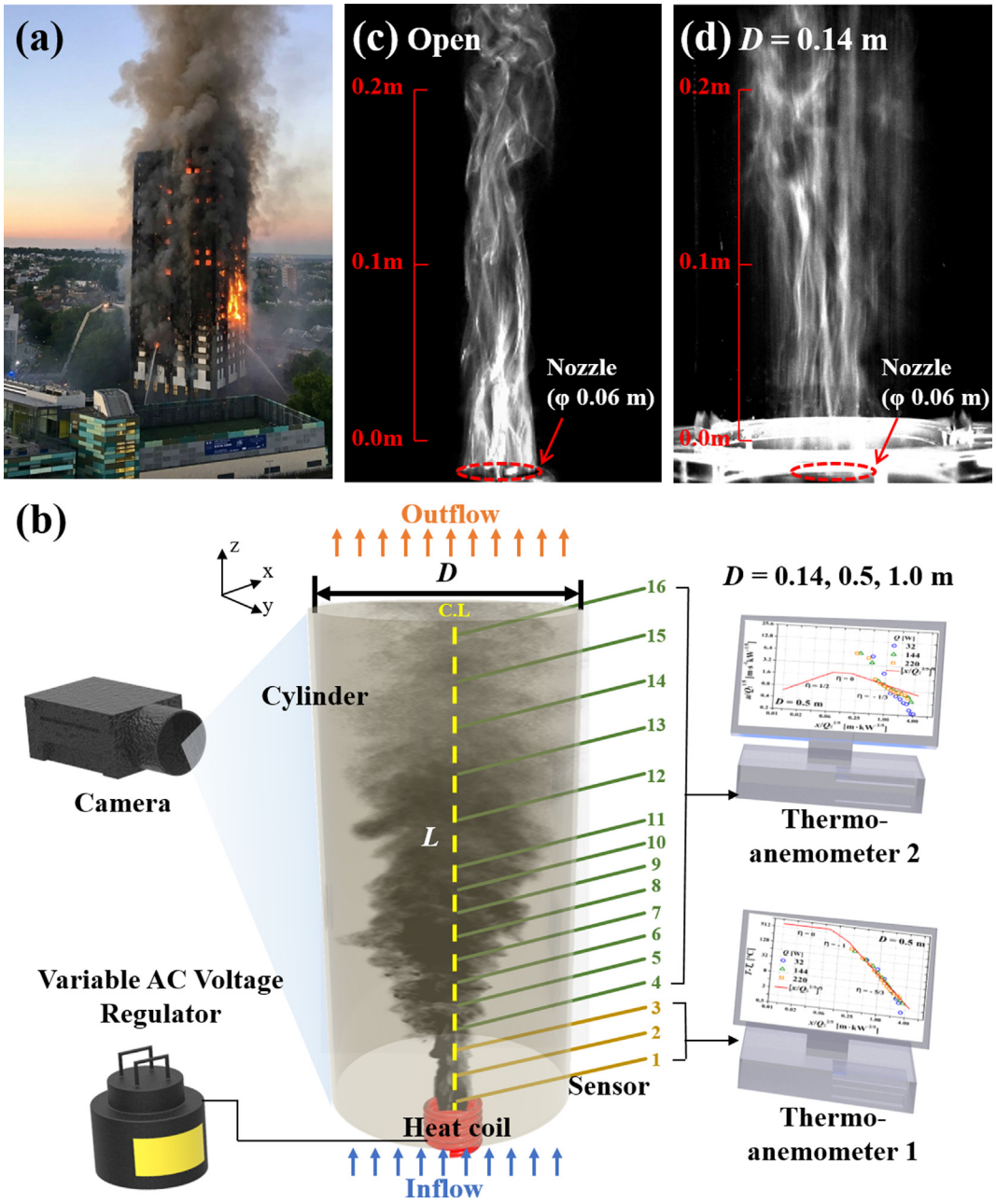

Fig. 1. (a) Illustration of a high-rise building fire. (b) Smoke plume from a pointwise source inside a cylinder instrumented with velocity and temperature probes. Plumes issuing from the smoke nozzle (c) in open air, and (d) in a cylinder of $D = 0.14$ m.

ambient pressure were between 0.50 and 0.62 of shaft height. Harish and Venkatasubbaiah [30] simulated flow patterns for varying shaft configurations and Grashof numbers. Their computations showed that periodic vortices shed from the compartment resulted in unsteady, chaotic shaft flows. Ji et al. [31] measured smoke temperatures and velocities at different floors within a stairwell. Qi et al. [32] presented a 1D analytical model for stack-effect smoke flow in a non-adiabatic shaft. Li et al. [33] presented experimental data and the corresponding 1D analytical model for the stack-effect flow in a stairwell. Ji et al. [34] experimentally measured the effects of different ventilation conditions on smoke dynamics in a stairwell attached to a compartment. Ji et al. [35] considered the influence of open windows on smoke behavior and the overall stack effect. These changes in the inlet and outlet boundary conditions significantly altered smoke dynamics and fuel burning rates. As for the counter-technologies against the stack effect, there are a few methods that have been implemented. First, physical barriers are installed along shafts that prevent any air/gas entrainment [36]. Second, a structure design with enhanced "air-tightness" is often introduced to mitigate the stack effect [37]. These first and second methods are considered as a passive control. As for an active control, the air pressure inside a structure is maintained high through mechanical pressurization [38]. Another alternative is to cool shafts directly to minimize the temperature difference in the longitudinal direction [39].

Here, smoke dynamics in a cylinder were studied to characterize the effects of the aspect ratio as well as viscous drag and heat loss through the walls. A threshold aspect ratio was identified where dramatically different smoke behavior from open-air conditions was observed. The fully developed turbulent flow achieved a

quasi-steady state from the smooth inflow through the cylinder bottom where the heat source was located. The physics behind the altered smoke dynamics at the threshold aspect ratio were described. Self-similar plume theory described the observed smoke dynamics in an open-air system. For the cylinder experiments, the Fire Dynamics Simulator (FDS) software assessed the wall effects on smoke dynamics and numerical results were verified against experimental data. This study was motivated by the need to acquire experimental data on smoke plumes in cylinders of different diameters to quantify wall effects. This simplified geometry yielded useful benchmark data that can be applied to study more complex structures such as elevators, ventilation shafts, and stairwells.

2. Theoretical and experimental approaches

Experiments were conducted in unconfined (open-air) and confined systems. Self-similar plume theory adequately describes unconfined plume characteristics; however, smoke dynamics were notably different for a plume confined to a narrow cylinder. As the diameter increased, plume behavior approached that of an open-air plume. Moreover, because the cylinder walls were not insulated, heat losses were important. First, plume theory is introduced and compared to the experiments to verify the data quality. Next, plume characteristics were measured in cylinders with three different diameters; $D = 1$, 0.5, and 0.14 m. Finally, these confined plumes were modeled with FDS to study the parameters governing smoke dynamics and to identify model limitations.

2.1. Plume jet theory

According to Yarin [40], for the axisymmetric turbulent plumes of interest here, the most important parameter governing flow is the released power Q_z (W), or its counterpart $Q_y = Q_z/(2\pi\rho c)$, where ρ and c are the density and specific heat at constant gas pressure, respectively. In an axisymmetric plume, the following relationship holds:

$$Q_y = \int_0^\infty u(y)[T(y) - T_\infty]y\mathrm{d}y, \tag{1}$$

where $u(y)$ is the longitudinal velocity profile as a function of the radial coordinate (y) in the plume, $T(y)$ is the longitudinal temperature distribution in the plume, T_∞ is the temperature of the surrounding gas; y is the radial coordinate in any plume cross-section reckoned from its axis (z is the longitudinal coordinate). Note that Q_y (and hence, Q_z) is constant along the plume, i.e., it does not depend on z and is thus, an input parameter.

The maximum axial cross-sectional velocity in a turbulent, axially symmetric plume is [40, the first Eq. (6.111)]:

$$u_{\max}(z) = \left(\frac{\beta g Q_z}{\rho c z}\right)^{1/3}, \tag{2}$$

where β is the thermal expansion coefficient of the gas, and g is gravitational acceleration.

Similarly, the axial distribution of the maximum temperature (i.e., the cross-sectional maximum) in a plume is [40, with a misprint correction in the second Eq. (6.111)]]:

$$T_{\max}(z) - T_\infty = \left(\frac{Q_z}{\rho c}\right)^{2/3} \frac{1}{(\beta g)^{1/3}} \frac{1}{z^{5/3}} \tag{3}$$

If a shaft provides air from intermediate floors to a rising plume, then the volumetric flow rate in the shaft will increase similarly to that of a free plume:

$$\dot{Q} = \int_0^\infty u(y)y\mathrm{d}y. \tag{4}$$

Combining (1)–(4), the self-similar solution yields

$$\dot{Q} = \left(\frac{\beta g Q_z}{\rho c}\right)^{1/3} z^{5/3} \times \text{constant}. \tag{5}$$

2.2. Fire dynamics Simulator

The FDS software (version 6.6.0) solved the Navier-Stokes equations for low-speed flows (Mach number < 0.3) [41], and it is appropriate for thermally driven plumes. Turbulence is described using large eddy simulation. Combustion is simulated using mixture-fraction analysis, which assumes instantaneous reaction of fuel and oxygen. In addition, radiation transport calculations are based on a non-scattering gray gas and wide-band model. The governing equations include continuity, momentum, and energy balances, species-concentration balances, and the ideal gas law [42]. A full description of the model was previously reported by the authors [43].

2.3. Experiments

The confined experimental setup consists of three open, acrylic cylinders with diameters $D = 1$, 0.5, and 0.14 m, heights $L = 2$ m, and wall thicknesses $t = 8$ mm as depicted in Fig. 1b. No cylinder was required for the open-air system. Each cylinder was instrumented with sensors spaced with $\Delta z = 0.1$ m from $z = 0$ to 1 m, and with $\Delta z = 0.2$ m from $z = 1$ to 2 m that measured temperatures and velocities along the smoke plume. Kanomax Model 0204 (Kanomax, Japan) was used at $z = 0.1$ and 0.2 m because this sensor measures temperatures up to 250 °C. All other sensors were Almemo FVAD 35 TH5Kx (Ahlborn, Germany). All temperature and velocity measurements were acquired along the centerline to capture the maximum velocity and temperature.

An electric heating coil was situated inside a 3-cm-long, 4-cm-diameter nozzle connected to a chamber containing burning incense. Heat from the burning incense was negligible compared to the supplied powers of 32, 144, and 220 W controlled with an AC voltage regulator that ranged from 80 to 220 V. Upon setting the heating power, 15 min was allowed to establish a steady state prior to measurements. Each test was repeated thrice and the results were averaged to yield the final temperatures and velocities. Ambient air temperature was $T_\infty = 24$ °C with a humidity level of about 30%.

3. Results and discussion

3.1. Effect of heating power

Fig. 2 shows the maximum smoke velocities and temperatures measured for $Q_z = 32$, 144, and 220 W in an open-air system and in cylinders with $D = 0.5$ and 0.14 m. Velocities varied with heating power because of the increase in buoyant forces. Temperatures also increased with Q_z because more thermal energy was supplied to the system. Data from the open-air experiment were also compared to the theoretical prediction from Eqs. (2) and (3) in Fig. 2a and b. The theoretical velocities were accurate for $z > 0.4$ m from the heat source, while theoretical temperatures were accurate for $z \geq 0.2$ m. As expected, the self-similar theory was accurate only at distances somewhat away from the thermal source for the velocities. The difference in the velocity prediction near the nozzle exit region also stems from the fact that in the experiment the velocity of the rising smoke is already non-zero at $z = 0$ m. Smoke at the nozzle exit ($z = 0$) is already in rising motion, which is initiated in the smoke generator below the nozzle exit plane. Smoke is generated and already accelerated by the heating coil below

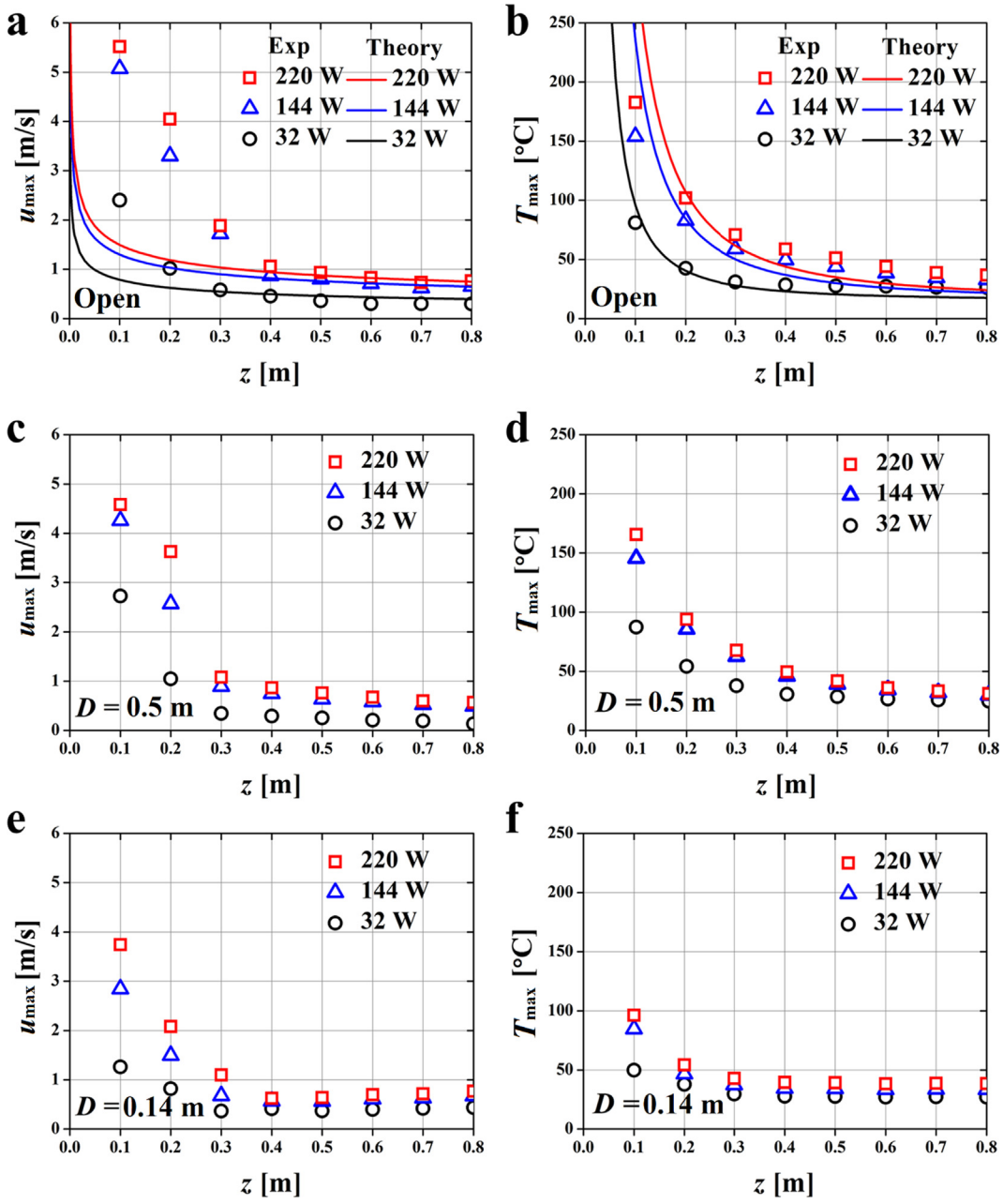

Fig. 2. Effect of Q_z on u_{max} and T_{max} for an open-air system (first row), and cylinders with $D = 0.5$ m (second row) and $D = 0.14$ m (third row).

$z = 0$ m, and thus, moving when exiting the nozzle exit; see Fig. 1c and d. Self-similar plume theory does not reflect this experimental peculiarity, and thus, underpredicts smoke velocity near the nozzle exit. Overall, the velocity comparison between the theory and experiment is excellent for $z > 0.4$ m for all heating powers. The theoretically predicted pattern also appears to be in agreement with the experimental data for different powers of 32, 144, and 220 W, as indicated in Fig. 2a.

3.2. Effect of cylinder diameter

Fig. 3 compares measured (symbols) u_{max} and T_{max} to the analytical predictions (curves) based on the self-similar plume theory for cylinders with $D = \infty$, 1, 0.5 and 0.14 m. As cylinder diameter D decreased (a more confining space), both velocities and temperatures decreased for all Q_z. Smoke velocities decreased because of the viscous boundary layer that developed along the cylinder walls; it spanned more of the radial distance as the cylinders narrowed. Smoke temperatures were reduced by heat losses through the cylinder walls.

In addition, when the cylinder diameter was narrower, the relative suction of the cold air at the cylinder bottom was enhanced and somewhat chaotic; see Fig. 1d. The reduced inlet cross-sectional area intensely drew in cold air from outside and enforced mixing with the rising hot smoke. The rising hot smoke was disturbed by the entraining cold air, and turbulent mixing occurred. As a result, the mixed air-smoke temperature was reduced at the centerline. When the cylinder diameter was larger, this type of mixing between cold-air and hot-smoke did not occur at the inlet; see Fig. 1c. The rising smoke was hardly disturbed and the plume dispersion versus height was as smooth as in a typical buoyant jet.

Fig. 4 compares T_{max} for the various cylinder diameters. Plotting the axial distance, z, divided by $Q_z^{2/5}$ on log-log plots as done by McCaffrey [7] collapsed the data onto a single fitting curve. Note

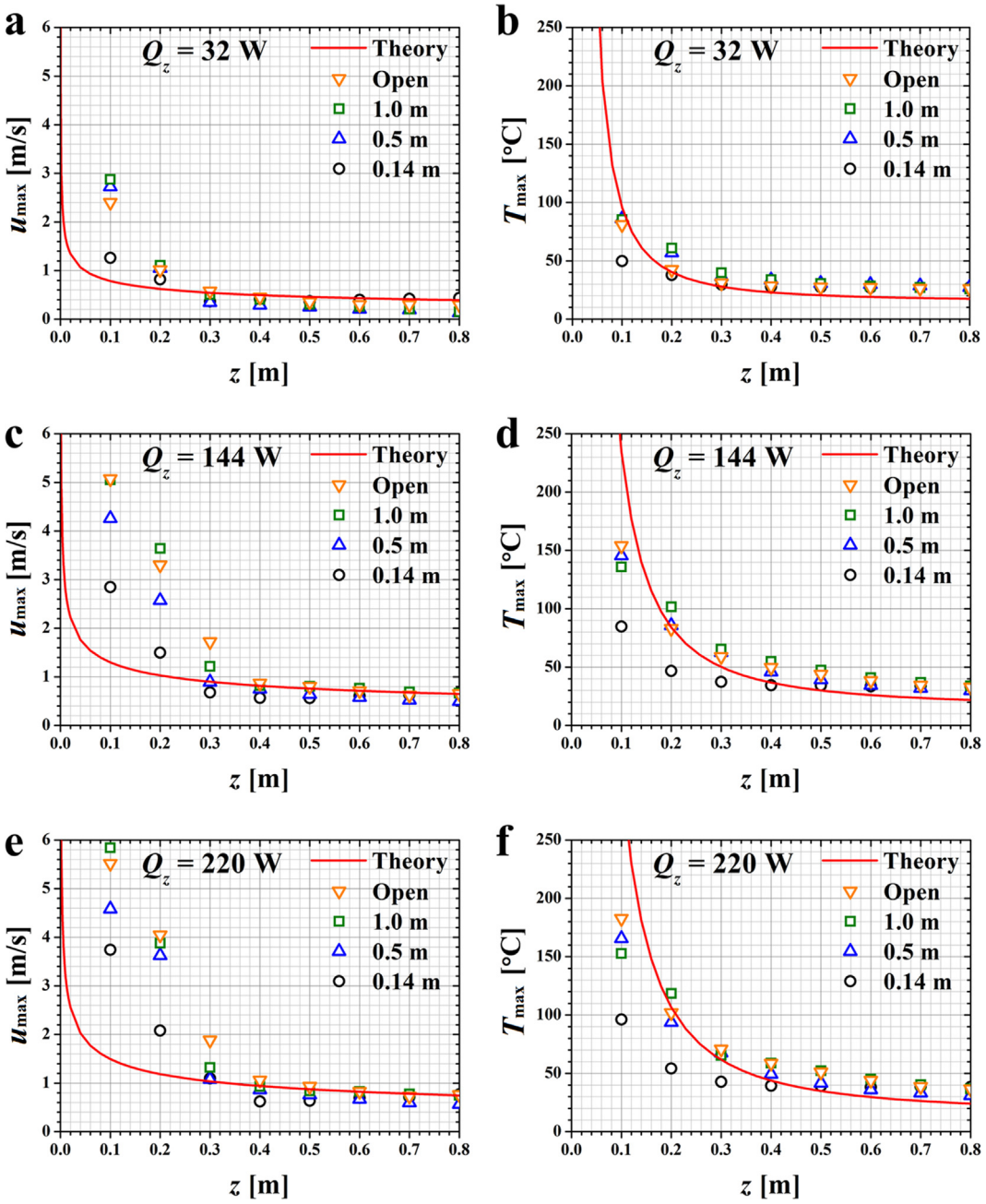

Fig. 3. Effects of cylinder diameter (D) on u_{max} and T_{max} for Q_z = 32 W (first row), Q_z = 144 W (second row), and Q_z = 220 W (third row).

that the empirical fit of McCaffrey [7] was derived for open-air conditions. The scaling exponents for the different slopes of the fitting curve are η = 0, −1, and −5/3, which correspond to the flame, intermittent, and plume (or smoke) zones, respectively. The scaling exponent −5/3 follows from the self-similar solution of Eq. (3), which is in perfect agreement in the plume zone data for $D = \infty$ and 0.5 m. Any deviation of the experimental data from the empirical fit, which coincides over this section with the self-similar solution of Eq. (3), would indicate the wall effect on the gas temperature T_{max}. Because such deviations are absent, Fig. 4a confirms the validity of both the self-similar theory and the empirical fit in the plume zone. Fig. 4b compares experimental data with the empirical fit for the open-air system. Agreement was generally good with some deviation for Q_z = 32 W near the cylinder exit. This deviation indicated that for low Q_z, measured temperature drop was slightly larger than the empirical fit prediction. In Fig. 4c, the experimental data for D = 0.5 m also collapses on the empirical fit, i.e., essentially, is described by the self-similar plume theory. For Q_z = 32 W near the cylinder exit, the experimental temperature drop was larger than the empirical fit prediction. Eventually, the value of $\Delta T = T_{max} - T_\infty$ nearly reaches $\Delta T \sim 0.01$ when $z/Q_z^{2/5} \sim 8$ (data not shown for clarity), indicating the smoke temperature is essentially reduced to the ambient temperature (T_∞) at $z/Q_z^{2/5} \sim 8$.

In Fig. 4d for D = 0.14 m, deviation of the experimental data from the empirical fit was evident for all Q_z due to wall effects in this narrow cylinder. Temperatures were affected by heat removal through the wall. Smoke temperatures were lower than the empirical fit for the open-air system when $z/Q_z^{2/5} \leq 1$, 1.5, and 3 for Q_z = 220, 144, and 32 W, respectively. The saturation of the temperature profile at larger z for D = 0.14 m means that in such a nar-

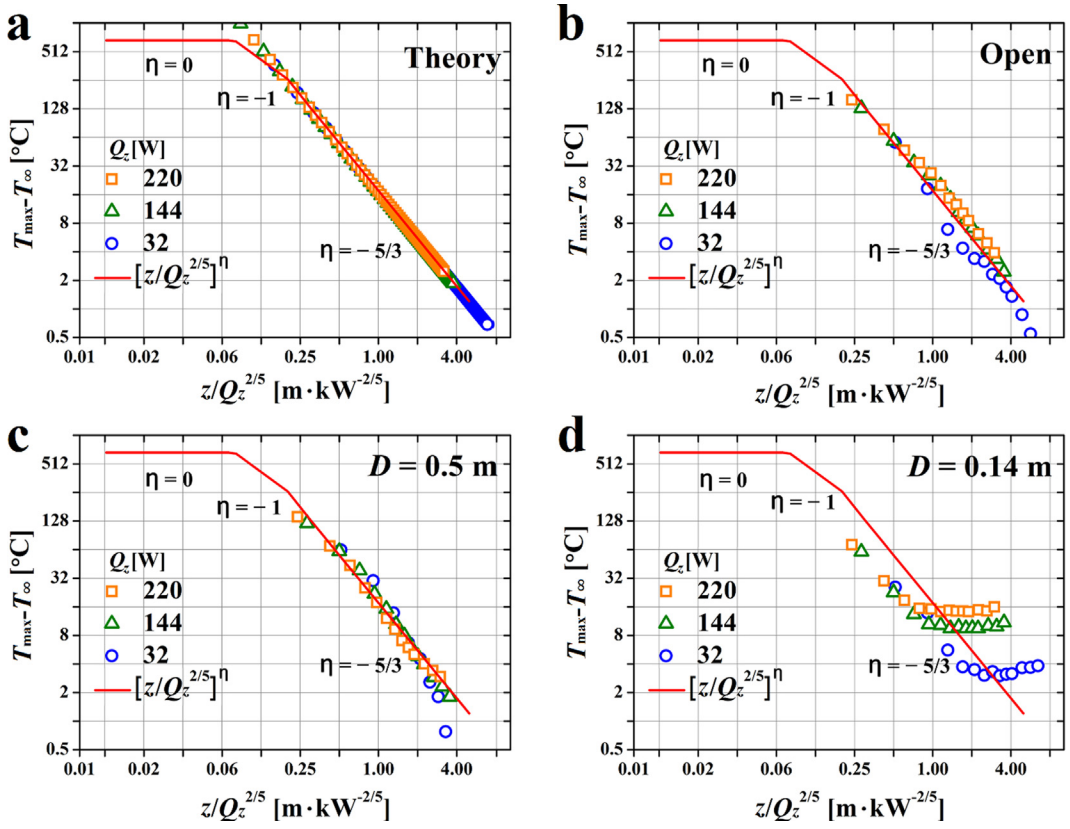

Fig. 4. Effect of shaft diameter (D) on the centerline maximum smoke temperature (T_{max}) for all heating powers (Q_z) compared with the empirical fit of McCaffrey [7] (solid line) on the log-log scale.

row pipe a fully-developed state is already reached for $Q_z = 220$, 144, and 32 W.

Fig. 5 compares the measured distribution of the maximum smoke velocity (u_{max}) along the axial direction (z) for different shaft diameters. The axial coordinate (z) is divided by $Q_z^{2/5}$ and the data is plotted on a log-log scale, which allowed McCaffrey [7] to collapse the data on a single fitting line for all heating powers (Q_z). Note that the empirical fit of McCaffrey [7] is valid only under the open-air conditions. The fitting scaling exponent $\eta = 1/2$, 0, and $-1/3$ corresponds to the flame, intermittent, and plume (or smoke) zones, respectively. Therefore, any deviation from the empirical fit, which coincides in the latter zone with the self-similar solution of Eq. (2), would indicate the wall effect on the centerline gas velocity u_{max}. The result in Fig. 5a does not reveal such deviations, and thus indicates no wall effect in this case. The comparison in the plume zone is good in the open air case (as expected). This comparison is still reasonable for $D = 0.5$ m, and fails in the narrow cylinder of $D = 0.14$ m.

Fig. 5b compares the experimental data with the empirical fit of McCaffrey [7] for the open-air case. The agreement is good, except in the region near the nozzle exit of $0.25 < z/Q_z^{2/5} < 1$. The experimentally measured velocities are higher than the ones from the fit for all cases ($Q_z = 32$, 144, and 220 W and $D = 0.14$, 0.5, 1 m, and ∞, which is an open air case) because smoke was supplied with a non-negligible velocity at the nozzle exit (see Fig. 1b), whereas the fit does not account for that. For $z/Q_z^{2/5} > 1$, the experimental data are in good agreement with the empirical fit of McCaffrey [7]. Also note that, in the open-air case, smoke is clearly moving even at the highest measuring location of $z/Q_z^{2/5} \sim 8$ for all values of Q_z, as indicated in Fig. 5b.

At smaller cylinder diameter (D), the smoke velocity was reduced because of the friction losses in the boundary layer; see Fig. 5c. The fit of McCaffrey [7] for open air does not account for these losses. This measured velocity deviation from the open-air fitting line begins in the $D = 0.5$ m case, especially for $Q_z = 32$ W, where the smoke velocity approaches zero at $z/Q_z^{2/5} \sim 8$ (not shown). When the cylinder is further narrowed to $D = 0.14$ m, the slowly rising smoke is prone to a slight increase in u_{max} while approaching the upper end of the cylinder when the data are presented in a log-log scale, as demonstrated in Fig. 5d. When the cylinder diameter is narrowed, the plume essentially becomes similar to a pipe flow and eventually reaches a fully-developed flow field. As a result, nearly a constant axial velocity u_{max} is found toward the end of the cylinder for all values of Q_z in Fig. 5d. However, when smoke exits the cylinder, u_{max} slightly reduces again to satisfy the continuity equation. Eventually, close to the highest axial location, the smoke motion slows down.

3.3. Numerical results

Convective heat fluxes were 45, 204, and 311 kW m^{-2} through the heat source with a 3-cm diameter corresponding to $Q_z = 32$, 144, and 220 W, respectively. A computational domain of $0.9 \times 0.9 \times 2$ m^3 with a computational mesh of $72 \times 72 \times 200$ (0.528 M nodes) was used. The smallest mesh size of $\Delta x = \Delta y = 0.00124$ m was used at the center; it was stretched to the boundary such that $\Delta x = \Delta y = 0.0354$ m. A uniform mesh was used in the axial direction with $\Delta z = 0.01$ m. All numerical data were time-averaged from $t = 20$ to 600 s to reflect steady-state conditions. The top and bottom surface of the domain were specified as open boundaries, except for the heat source. No-slip and thermal-insulation boundary conditions were imposed along the cylinder wall.

Fig. 6 compares the experimental images of the rising smoke in open-air plumes compared with the numerically predicted temperature fields at the corresponding heating power. As the heating

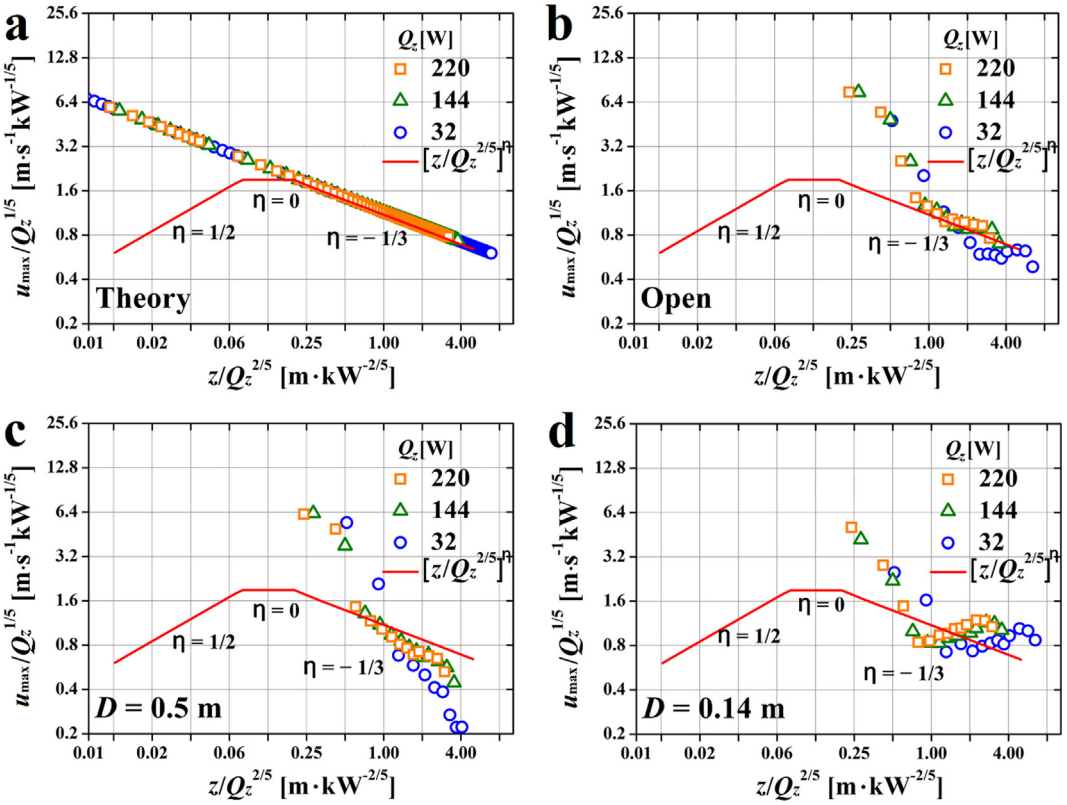

Fig. 5. Effect of shaft diameter (D) on smoke velocity (u_{max}) for all heating powers (Q_z). compared with the empirical fit of McCaffrey [7] on a log-log scale.

power increases, the smoke jet visibly extends to a greater height because of a higher buoyancy force induced by greater heating power. The jet widths are also larger for the increased heating power, as is seen in the experimental images and corroborated by numerical simulations. Note that some differences between the experimental and numerical results are observed near the smoke nozzle exit, $z = 0$ m. The experimental images show narrow plumes at least up to $z = 0.3$ m, which significantly widen after that. In the numerical simulations, the air flow was thermally induced by the heat source located at $z = 0$ m and there was no nozzle that feeds smoke from below $z = 0$ m. The numerical predictions show an almost immediately widening plume. The difference stems from the fact that a converging nozzle 'focuses' the flow, the effect which dominates the thermal expansion up to $z = 0.3$ m. The numerical results do not account for the nozzle-driven flow convergence, and reveal plume widening immediately. It should be emphasized that the experimental and numerical plume widths rapidly become similar at z = 0.3 m, when the effect of the nozzle fades.

Fig. 7 compares the numerical predictions of the velocity and temperature fields in the rising smoke plumes at different heat source powers, and under different boundary conditions: without or with encasing cylinders of different sizes. As the smoke rises, both the axial velocity and temperature decrease for all values of D because of the friction losses and cooling. In the open-air case ($D = \infty$), the width of the rising smoke is increased at increasing Q_z. At smaller cylinder diameters, uniformity of both velocity and temperature cross-sectional profiles is increased in the axial direction as the smoke flow approaches to the fully-developed state. In Fig. 7c, the impression is that the velocity is practically uniform over the entire cylinder, but the temperature distribution suggests that the flow is still not fully uniform in the axial direction when $D = 0.14$ m and $Q_z = 220$ W.

3.4. Comparison of FDS simulations to experimental data

Fig. 8 compares the experimental data for the axial velocity and temperature with the numerical predictions for $Q_z = 144$ W at different cylinder diameters D. Once again, the predicted velocity differs significantly from the experimental data near the smoke nozzle region (where the conditions are different in both cases), whereas the overall temperature distributions are in excellent agreement. Further from the origin, velocity and temperature distributions found experimentally, numerically, or via the empirical fit of McCaffrey [7] are in excellent agreement in the open-air case in Fig. 8a.

For the cylinder diameter of $D = 0.5$ m, deviation of the experimental, numerical, and empirical results become visible in Fig. 8b. The deviations of the data and numerical results from the empirical line indicate the importance of the wall effect. Along the plume, the reduction in the experimental velocity is more prominent than that in the numerical results. In conjunction with Figs. 4c and 5c, both temperature and velocity are in reasonable agreement with the open-air case when $D = 0.5$ m, which indicates that the wall effect at $D = 0.5$ m is not very significant at least when $Q_z = 144$ W. However, the numerical simulations underestimate the wall effect and the axial velocity practically ceases to decrease in the narrow cylinder of diameter $D = 0.14$ m (cf. Fig. 8c, left). This is reminiscent of Fig. 7b (see the $D = 0.14$ m case in the velocity distribution). The underestimation of the wall effect in the numerical simulations may stem from the assumption of a perfectly adiabatic wall. However, in reality, the wall has a finite thickness through which heat does transfer both vertically and horizontally. Therefore, this is essentially a conjugate heat transfer problem in which both convection in the cylinder, as well as conduction in its wall play a discernable role in affecting the flow. Given that the wall was made of acryl having the thermal conductivity of 0.2 W/m-K

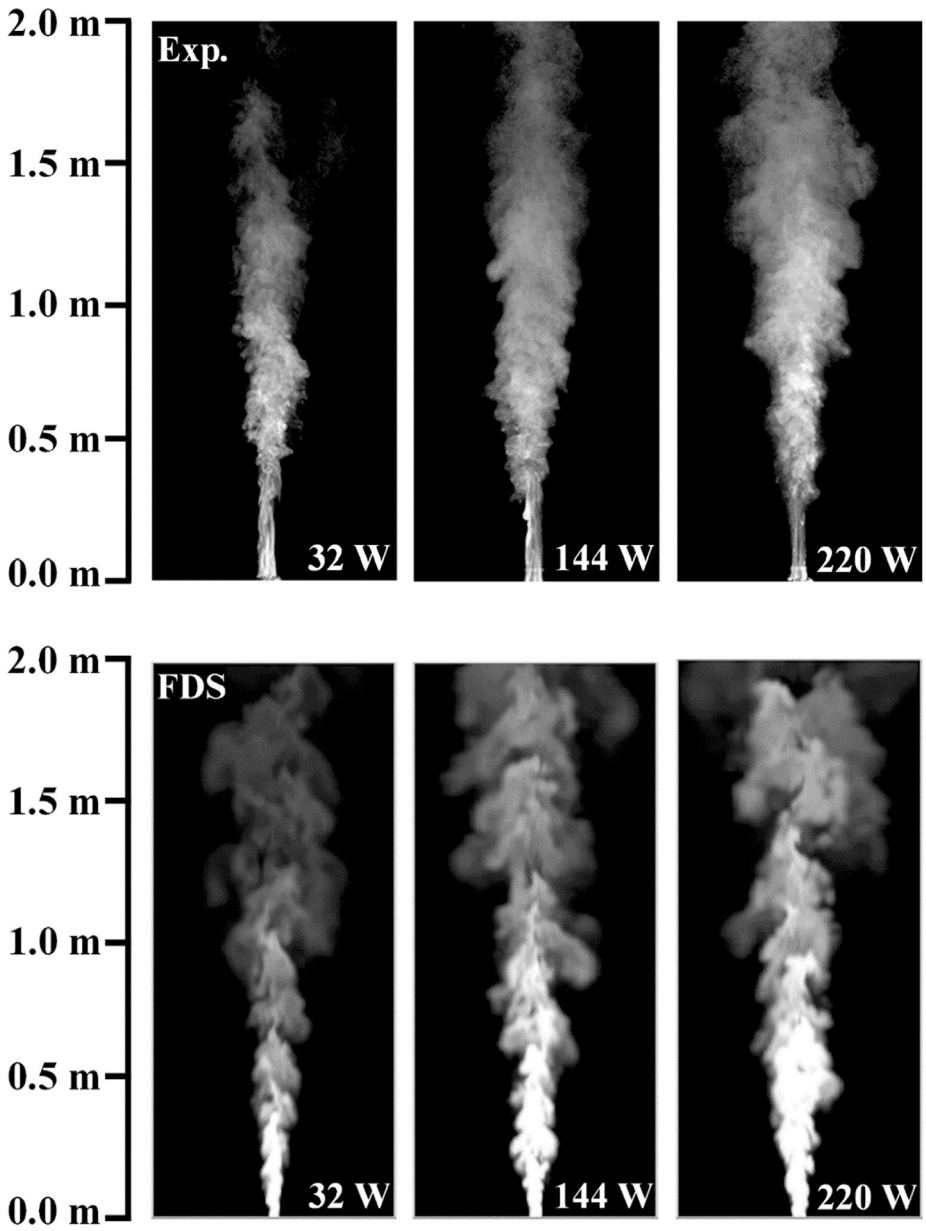

Fig. 6. Snapshots of rising smoke plumes in the open-air system for the indicated Q_c values. First row: experiment, second row: temperature distribution in a grey scale predicted using Fire Dynamics Simulator.

(as opposed to that of air, which is 0.02 W/m-K), conduction along the wall does not seem to be negligible. This thermal conduction effect would become more important for a narrower cylinder where thermal convection is diminished. As a result, the wall does heat up and may provide an additional heat source that renders a slight velocity increase at the cylinder top (or exit). For this reason, in the experiment in the narrow cylinder, velocity even increases for a while, and then decreases once more near the cylinder exit (cf. Fig. 8c, left). On the other hand, the temperature distribution measured experimentally and predicted numerically are in excellent agreement when $D = 0.14$ m; see Fig. 8c (right).

4. Conclusion

Smoke rise in open air and cylinders of different diameter driven by buoyancy associated with a heat source at the entrance is studied experimentally, analytically and numerically (using FDS). The experimental data obtained for a turbulent plume in open air was adequately described analytically by the self-similar solution, as well as numerically by FDS. When the aspect ratio (diameter D to length L) of the cylinder is $D/L \geq 0.25$, the buoyancy-driven smoke flow resembles a turbulent plume rising in open air. When the aspect ratio is $D/L = 0.07$, the viscous friction at the wall slowed the smoke velocity. For $D/L = 0.07$, the axial velocity of smoke was numerically predicted to plateau; probably the code underestimated the wall effect under the imposed adiabatic conditions. In the experiment, the axial velocity even slightly increased over a certain section, which was followed by a decrease once again. The deviations between the experimental data and modeling results are the most pronounced near the heat source where the conditions were different. The self-similar and numerical solutions imply a fully thermally-driven smoke motion starting from the source, i.e., pure natural convection, whereas in the experiment

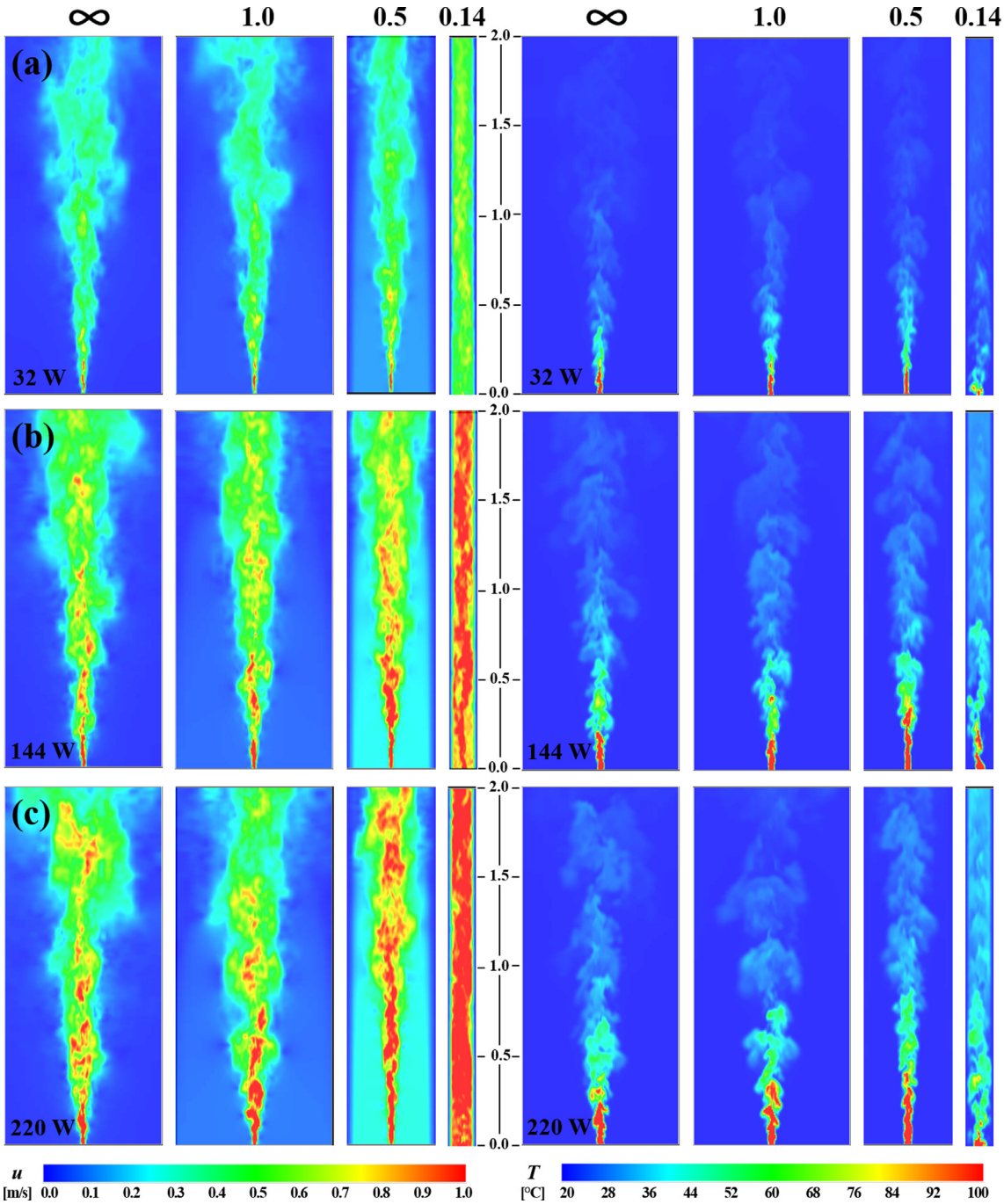

Fig. 7. FDS numerical simulations of the smoke-plume longitudinal velocity and temperature inside the encasing shafts of different sizes: open air ($D = \infty$), and D = 1, 0.5, and 0.14 m. The heating power is (a) Q_z = 32 W, (b) 144 W, and (c) 220 W.

smoke was supplied from a nozzle with a non-negligible forced convection.

The present work deals with a model, most simplistic situation, which allows one to elucidate the main physical mechanisms. The real smoke fire scenarios in some cases involve more complex and cluttered obstacles inside buildings. However, there are simple structures which do not possess obstacles within a shaft, the examples of which may be an elevator shaft or/and ventilation hollow structures. The fundamental studies of the smoke dynamics in a hollow structure may provide an insight relevant for all cases. The smoke dynamics involving more complex internal structures will be studied in future. One of such cases would be pure natural convection or mixed natural and forced convection flows in vertical shafts and pipes heated from one side and closed on the top (an ultimately blocked case) where smoke is entrained into a circulatory flow: rising on the heated side and descending on the cooler one.

Conflict of Interest

The authors declared that there is no conflict of interest.

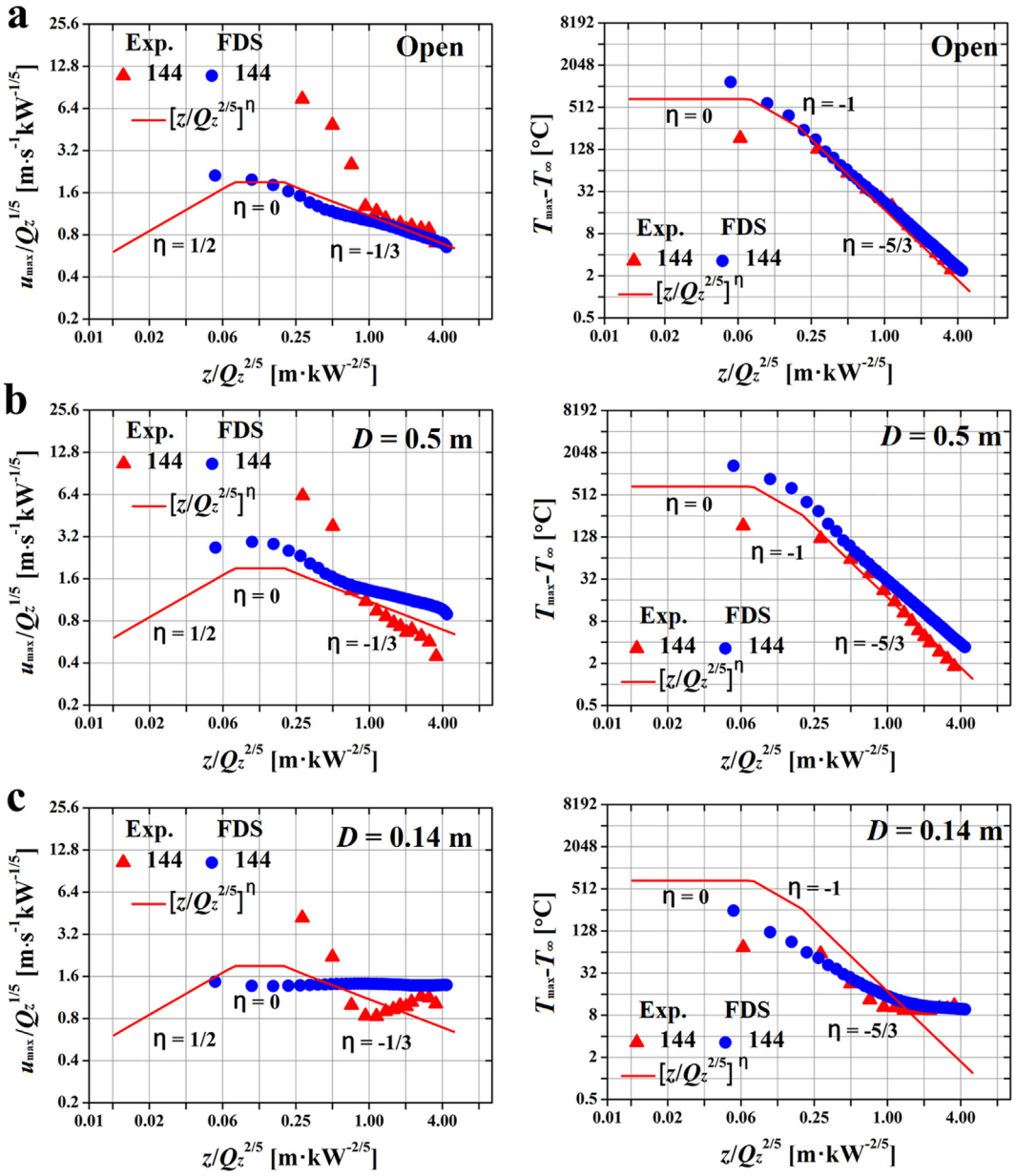

Fig. 8. Velocity and temperature distributions: comparison between the experimental (triangles) and numerical (circles) results for Q_z = 144 W. The lines show the McCaffrey's empirical correlation.

Acknowledgement

This work was supported by the National Research Council of Science & Technology (NST) grant by the Ministry of Science and ICT (No. CRC-16-02-KICT), Advanced Research Center Program (NRF-2013R1A5A1073861, and NRF-2016M1A2A2936760) of the South Korea government.

References

[1] Y.B. Zeldovich, Limiting laws of freely rising convection currents, Zhurnal Eksperimentalnoii Teoreticheskoy Fizika 7 (1937) 1463–1465.
[2] B. Morton, G. Taylor, J. Turner, Turbulent gravitational convection from maintained and instantaneous sources, in: Proceedings of the Royal Society of London A: Mathematical, Physical and Engineering Sciences, The Royal Society, 1956, pp. 1–23.
[3] S. Yokoi, Study on the prevention of fire-spread caused by hot upward current, Rep. Build. Res. Inst. 34 (1960) 1–118.
[4] B. Morton, Modeling fire plumes, in: Symposium (International) on Combustion, Elsevier, 1965, pp. 973–982.
[5] J. Turner, Buoyant plumes and thermals, Annu. Rev. Fluid Mech. 1 (1) (1969) 29–44.
[6] W.K. George, R.L. Alpert, F. Tamanini, Turbulence measurements in an axisymmetric buoyant plume, Int. J. Heat Mass Transf. 20 (11) (1977) 1145–1154.
[7] B. McCaffrey, Purely buoyant diffusion flames: Some experimental results, in: Final Report, Chemical and Physical Processes in Combustion, The National Institute of Standards and Technology (NIST), Miami Beach, 1979, p. 49.
[8] G. Heskestad, Peak gas velocities and flame heights of buoyancy-controlled turbulent diffusion flames, in: Symposium (International) on Combustion, Elsevier, 1981, pp. 951–960.
[9] H.-C. Kung, P. Stavrianidis, Buoyant plumes of large-scale pool fires, in: Symposium (International) on Combustion, Elsevier, 1982, pp. 905–912.
[10] G. Heskestad, Luminous heights of turbulent diffusion flames, Fire Saf. J. 5 (2) (1983) 103–108.
[11] G. Heskestad, Engineering relations for fire plumes, Fire Saf. J. 7 (1) (1984) 25–32.
[12] J.G. Quintiere, Scaling applications in fire research, Fire Saf. J. 15 (1) (1989) 3–29.
[13] J. Quintiere, B. Grove, A unified analysis for fire plumes, in: Symposium (International) on Combustion, Elsevier, 1998, pp. 2757–2766..
[14] Y. Wang, P. Chatterjee, J.L. de Ris, Large eddy simulation of fire plumes, Proc. Combust. Inst. 33 (2) (2011) 2473–2480.

[15] F. Tang, L. Hu, Z. Qiu, Q. Wang, A global model of plume axial temperature profile transition from axisymmetric to line-source pool fires in normal and reduced pressures, Fuel 130 (2014) 211–214.
[16] X. Zhang, L. Hu, W. Zhu, X. Zhang, L. Yang, Axial temperature profile in buoyant plume of rectangular source fuel jet fire in normal-and a sub-atmospheric pressure, Fuel 134 (2014) 455–459.
[17] W. Baines, J. Turner, Turbulent buoyant convection from a source in a confined region, J. Fluid Mech. 37 (1) (1969) 51–80.
[18] M.G. Worster, H.E. Huppert, Time-dependent density profiles in a filling box, J. Fluid Mech. 132 (1983) 457–466.
[19] S.J. Barnett, The Dynamics of Buoyant Releases in Confined Spaces, University of Cambridge, 1992.
[20] S.S. Cardoso, A.W. Woods, Mixing by a turbulent plume in a confined stratified region, J. Fluid Mech. 250 (1993) 277–305.
[21] M. Wells, R. Griffiths, J. Turner, Competition between distributed and localized buoyancy fluxes in a confined volume, J. Fluid Mech. 391 (1999) 319–336.
[22] K. Moinuddin, G. Thorpe, N. George, A. Ooi, I. Marusic, D. Chung, Direct numerical simulation of a turbulent line plume in a confined region, in: Proceedings of the 20th Australasian Fluid Mechanics Conference, Australasian Fluid Mechanics Society, 2016, pp. 1–23.
[23] X. Gao, A. Li, C. Yang, Study on thermal stratification of an enclosure containing two interacting turbulent buoyant plumes of equal strength, Build. Environ. 141 (2018) 236–246.
[24] L.Y. Cooper, Simulating smoke movement through long vertical shafts in zone-type compartment fire models, Fire Saf. J. 31 (2) (1998) 85–99.
[25] S.Y. Kim, Y. Jaluria, Basic considerations in combined buoyancy-induced and forced flow in a vertical open shaft, Num. Heat Transfer, Part A Appl. 34 (5) (1998) 519–536.
[26] G. Mercier, Y. Jaluria, Fire-induced flow of smoke and hot gases in open vertical enclosures, Exp. Therm Fluid Sci. 19 (2) (1999) 77–84.
[27] J.G. Quintiere, Fire behavior in building compartments, Proc. Combust. Inst. 29 (1) (2002) 181–193.
[28] J. Zhang, J. Ji, R. Huo, H. Yuan, R. Yang, A comparison of simulation and experiment on stack effect in long vertical shaft, J. Fire Sci. 24 (2) (2006) 121–135.
[29] J. Zhang, W. Lu, R. Huo, R. Feng, A new model for determining neutral-plane position in shaft space of a building under fire situation, Build. Environ. 43 (6) (2008) 1101–1108.
[30] R. Harish, K. Venkatasubbaiah, Transport phenomena of turbulent fire spread through compartment connected to vertical shaft in tall building, Fire Saf. J. 61 (2013) 160–174.
[31] J. Ji, L. Li, W. Shi, C. Fan, J. Sun, Experimental investigation on the rising characteristics of the fire-induced buoyant plume in stairwells, Int. J. Heat Mass Transf. 64 (2013) 193–201.
[32] D. Qi, L. Wang, R. Zmeureanu, An analytical model of heat and mass transfer through non-adiabatic high-rise shafts during fires, Int. J. Heat Mass Transf. 72 (2014) 585–594.
[33] L. Li, J. Ji, W. Shi, Z. Gao, J. Sun, J. Zhu, A modified turbulent mixing model with the consideration of heat transfer between hot buoyant plume and sidewalls in a closed stairwell, Int. J. Heat Mass Transf. 84 (2015) 521–528.
[34] J. Ji, M. Li, Z. Gao, Y. Li, W. Shi, J. Sun, Experimental investigation of combustion characteristics under different ventilation conditions in a compartment connected to a stairwell, Appl. Therm. Eng. 101 (2016) 390–401.
[35] J. Ji, M. Li, W. Shi, Z. Gao, J. Sun, S. Lo, Deflection characteristic of flame with the airflow induced by stack effect, Int. J. Therm. Sci. 115 (2017) 160–168.
[36] J. Lee, T. Hwang, D. Song, J.T. Kim, Quantitative reduction method of draft in high-rise buildings, using revolving doors, Indoor Built Environ. 21 (2012) 79–91.
[37] R. Kosonen, J. Jokisalo, I. Ranta-aho, E.-P. Koikkalainen, Methods to reduce stack effect and improve energy efficiency in a Nordic high rise residential building, Procedia Eng. 205 (2017) 2311–2317.
[38] J.-Y. Yu, K.-D. Song, D.-W. Cho, Resolving stack effect problems in a high-rise office building by mechanical pressurization, Sustainability 9 (2017) 1731.
[39] D.-R. Park, J.-H. Lee, D.-S. Song, A study on the reduction strategies of stack effect in high-rise residential buildings, in: Proceedings of the SAREK, 2007, pp. 546–552.
[40] L.P. Yarin, The Pi-Theorem: Applications to Fluid Mechanics and Heat and Mass Transfer, Springer-Verlag, Berlin, Heidelberg, 2012.
[41] K. McGrattan, S. Hostikka, R. McDermott, J. Floyd, C. Weinschenk, K. Overholt, Fire dynamics simulator user's guide, NIST Spe. Publ. 1019 (2013), 6th edition.
[42] R.G. Rehm, H.R. Baum, The equations of motion for thermally driven, buoyant flows, J. Res. NBS 83 (297–308) (1978) 2.
[43] K.B. McGrattan, H.R. Baum, R.G. Rehm, A. Hamins, G.P. Forney, J.E. Floyd, S. Hostikka, K. Prasad, Fire Dynamics Simulator–Technical Reference Guide, National Institute of Standards and Technology, Building and Fire Research Laboratory, 2000.